Eur. Phys. J. B **19**, 177–184 (2001)

THE EUROPEAN PHYSICAL JOURNAL B

EDP Sciences
© Società Italiana di Fisica
Springer-Verlag 2001

Electronic and magnetic properties of ruthenocuprates

B.H. Frazer[1], Y. Hirai[1], M.L. Schneider[1], S. Rast[1], M. Onellion[1,a], I. Nowik[2], I. Felner[2], S. Roy[3], N. Ali[3], A. Reginelli[4], L. Perfetti[4], D. Ariosa[4], and G. Margaritondo[4]

[1] Physics Department, University of Wisconsin, Madison, WI, USA
[2] Racah Institute of Physics, Hebrew University, Jerusalem, Israel
[3] Physics Department, Southern Illinois University, Carbondale, IL, USA
[4] Institute of Applied Physics, EPFL, 1024 Lausanne, Switzerland

Received 23 August 2000

Abstract. We report on X-ray photoemission of core levels, valence band studies using angle-integrated photoemission, and magnetization measurements of ruthenocuprate and $SrRuO_3$ polycrystalline samples. The data indicate that the RuO_2 planes are the source of the energetics of the magnetic ordering. We also find that adding hydrogen leads to changes in the many-body response on both the CuO_2 and EuO planes.

PACS. 74.72.Jt Other cuprates – 74.70.-b Superconducting materials (excluding high-T_c compounds) – 74.25.Ha Magnetic properties – 75.50.-y Studies of specific magnetic materials

Introduction

In the past few years, several reports of ruthenocuprate samples indicate a new way to investigate the competition and possible coexistence of ferromagnetism and superconductivity [1–8]. One fundamental reason for such studies is that superconductivity leads to a macroscopic coherent quantum state. If the material has ferromagnetic layers interspersed between superconducting layers, how can phase coherence of the superconducting state be maintained between the layers?

The ruthenocuprate samples include CuO_2 and RuO_2 planes in the unit cell. There is some evidence that the RuO_2 layers participate in some type of long range magnetic order [2–5]. It is widely believed, but so far without conclusive evidence, that the CuO_2 planes are the source of the superconductivity. Because there are RuO_2 planes and planes containing rare earth nuclei between each CuO_2 planes, this is an excellent model system to investigate the relationship between superconductivity and ferromagnetism.

Our main result is that the RuO_2 planes do indeed seem the source of the energetics involved in the magnetic phase transition. The main electronic states, near the chemical potential, that are involved in the magnetic phase transition are predominantly oxygen in origin. For metallic ruthenocuprates, the other planes in the unit cell resemble cuprate and insulating rare earth and alkaline earth planes, consistent with the charge reservoir idea in the cuprates. However, for hydrogen loaded samples, we find that both the CuO_2 and EuO planes exhibit a different many-body response – and this response changes across the magnetic phase transition. After presenting the data to substantiate these points, we suggest a consistent picture of the interactions involved. At the same time, it is important to note that we do not have definitive evidence on how the change from metallic to insulating (hydrogen loaded) ruthenocuprates affects the magnetic properties.

Experimental

Polycrystalline samples of $SrRuO_3$, $Eu_{1.5}Ce_{0.5}Sr_2RuCu_2O_{10-\delta}$ (Eu-2212) and $EuSr_2RuCu_2O_{8-\delta}$ (Eu-1212) were prepared by solid state reaction of CeO_2, Eu_2O_3, Ru, and $SrCO_3$. Precursor powders were ground, pressed and then fired at 1000 °C for 24 hours in air. The material was then reground, pressed and fired in 1atm of O_2, at 1050 °C, for 72 hours. Hydrogen-loaded $Eu_{1.5}Ce_{0.5}Sr_2RuCu_2O_{10-\delta}$ (Eu-2212+H) samples were prepared by annealing the samples in a fixed volume of several atmospheres of hydrogen [3,4]. The samples were made in two laboratories and extensively characterized using XRD, AC susceptibility, DC magnetization, and resistivity [1–9]. Eu-2212 samples were verified to be superconducting with transition temperature ∼39 K by diamagnetic response and by zero resistivity. These samples are also weak ferromagnets, as confirmed by both SQUID magnetometry and AC susceptibility, and have a Curie temperature of approximately 120 K. Eu-1212 samples do not exhibit superconductivity, but appear to show ferromagnetic behavior with a Curie temperature of about 150 K. Eu-2212+H samples exhibit some type of long-range magnetic order with an ordering temperature of approximately 180 K. All data presented have been carefully and repeatedly reproduced. Further

[a] e-mail: onellion@comb.physics.wisc.edu

details are reported elsewhere [9]. X-ray Photoemission Spectroscopy (XPS) measurements were performed with a Scienta ESCA 300 electron energy analyzer and an Al rotating anode photon source.

Results

We performed extensive X-ray photoemission spectroscopy measurements, using an AlKα source of 1486.6 eV photons, which included measurements from the chemical potential to a binding energy of 1180 eV. We present data in the following order: Eu3d region; Sr3d region; Sr3p and Ru3d region; Ru3p region; Cu2p region; binding energy of 10–100 eV region; valence band.

Eu3d region

Previous authors have reported on studying the Eu3d core level in both metallic and insulating environments [10,11] and on the Eu response to another layer that orders magnetically [12]. As illustrated in Figure 1, between 1110–1180 eV binding energy, there is a single doublet, due to the Eu3d state, for the Eu-2212 (upper) and Eu-1212 (bottom) samples. The doublet is at the same binding energy for both samples, and both the binding energy and spectral intensity are almost independent of temperature. The data indicate that (Eu) is in the (+3) valence state; note the absence of a feature at ∼1124 eV binding energy [13]. The superconducting sample exhibits a small multiplet structure at ∼1142 eV binding energy. The overall lineshape is an excellent match to the calculated multiplet structure of trivalent Eu having a ($3d4f^6$) configuration [14] and to EuF_3, $EuCl_3$ and Eu_2O_3 compounds [13]. The Eu-1212 ruthenocuprate exhibits a similar spectrum, except that the multiplet structure at ∼1142 eV is not clearly observed.

By contrast, for the Eu-2212+H sample (middle), the Eu is again in the (+3) valence state. The multiplet structure is markedly different from that of the metallic ruthenocuprates, but is virtually identical to the (+3) valence part of $EuPd_2P_2$ and EuSi [11]. As reference [11] discussed, the multiplet of $EuPd_2P_2$ and EuSi arises from the many-body response in the photoemission final state to the core photohole. The multiplet structure we observe for the Eu-2212+H sample is quite different from the insulating Eu compounds reported in reference [10]. We return to this point below.

Ru3p region

As Figure 2 illustrates, between 455–495 eV binding energy, there is a single doublet, due to the Ru3p state, for the Eu-2212 (upper), Eu-1212 (middle) and $SrRuO_3$ (bottom) samples. The spectra for the metallic samples is normalized with the (small) background subtracted. The

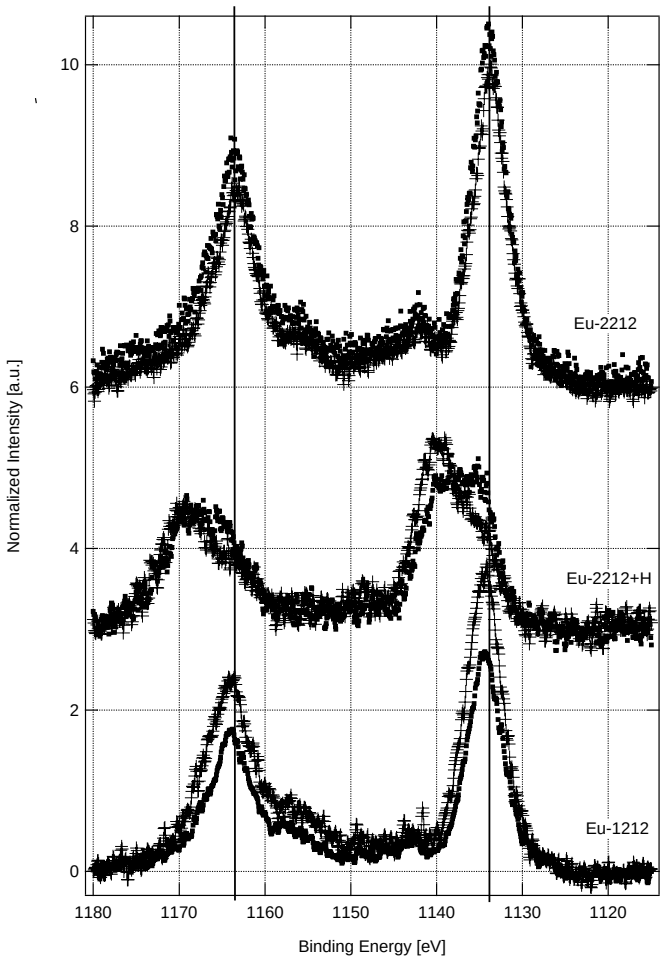

Fig. 1. Angle-integrated photoemission spectra taken using photon energy of 1486.6 eV. Spectra at room temperature (closed square) and 80 K (cross) illustrated. Top: Superconducting ruthenocuprate (Eu-2212); Middle: Eu-2212+H; Bottom: Magnetic ruthenocuprate (Eu-1212). Eu3d core level visible.

binding energies and peak intensities are temperature independent for all three metallic samples. Both metallic ruthenocuprate samples exhibit a binding energy ∼0.6 eV higher than the $SrRuO_3$.

Cu2p region

Figure 3 illustrates X-ray photoemission data taken across the Cu2p core level region, including (top) the Eu-2212 ruthenocuprate, (middle) the Eu-2212+H, and (bottom) the Eu-2212. Several points emerge directly from the data as illustrated in Table 1.

Sr3d region

Figure 4 illustrates the binding energy range of 127–138 eV, which includes the Sr3d core level. The Eu-1212 (upper), Eu-2212 (second), Eu-2212+H (third)

Table 1. Summary of figure three analysis, including data taken at 300 K and at 80 K. All notation follows reference [20]. $E_s - E_m$ (eV) is the difference in satellite (s) and main peak (m) binding energy for the Cu2$p_{3/2}$ state. (I_s/I_m) is the ratio of satellite to main peak integrated intensity. These are both measured quantities. (U_{cd}) is the repulsive interaction between the $2p$ core hole and the $3d$ hole of the $3d^9$ configuration, (T) the d-ligand hybridization, and (Δ) the charge transfer energy, all calculated using the Anderson Hamiltonian model following references [20] and [26].

Material	Temp.	$E_s - E_m$ (eV)	I_s/I_m	U_{cd} (eV)	T (eV)	Δ (eV)
Eu-2212	300 K	9.0	0.33	7.8	2.3	0.4
	80 K	9.0	0.33	7.8	2.3	0.4
Eu-1212	300 K	9.0	0.43	7.8	2.3	0.4
	80 K	9.0	0.43	7.8	2.3	0.4
Eu-2212 + H	300 K	4.6	2.2	4.8	1.2	[0.4–1.0]
	80 K	6.1	2.1	6.0	1.5	[0.4–1.0]
$YBa_2Cu_3O_x$ (Ref. [20])		8.8	0.33	7.8	2.5	0.4
CuO (Ref. [20])		8.9	0.45	8.4	2.4	1.0

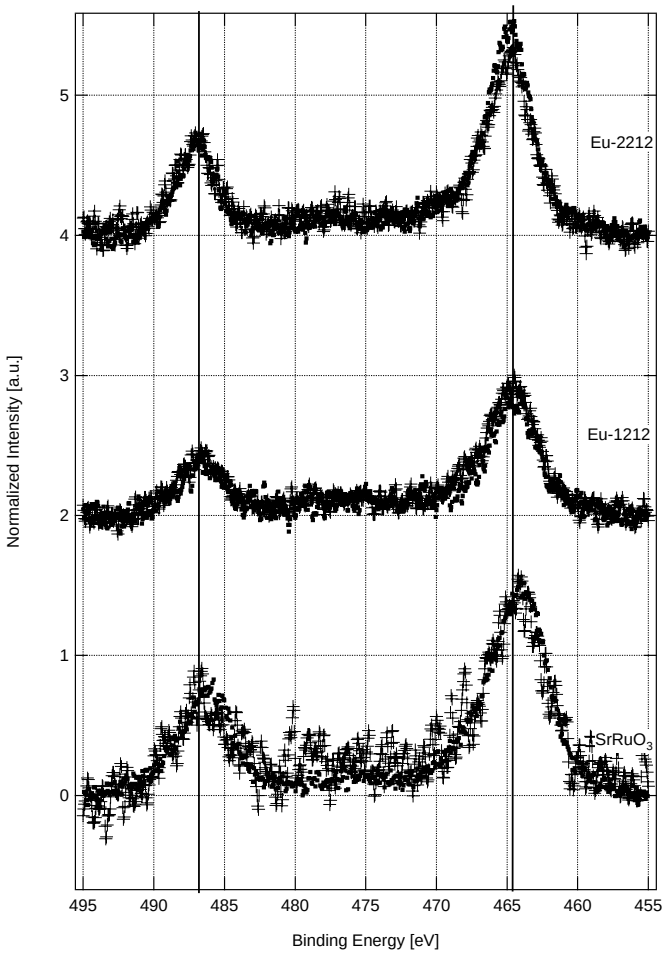

Fig. 2. Angle-integrated photoemission spectra taken using photon energy of 1486.6 eV. Spectra at room temperature (closed square) and 80 K (cross) illustrated. Top: Eu-2212; Middle: Eu-1212; Bottom: $SrRuO_3$. Ru3p core level visible.

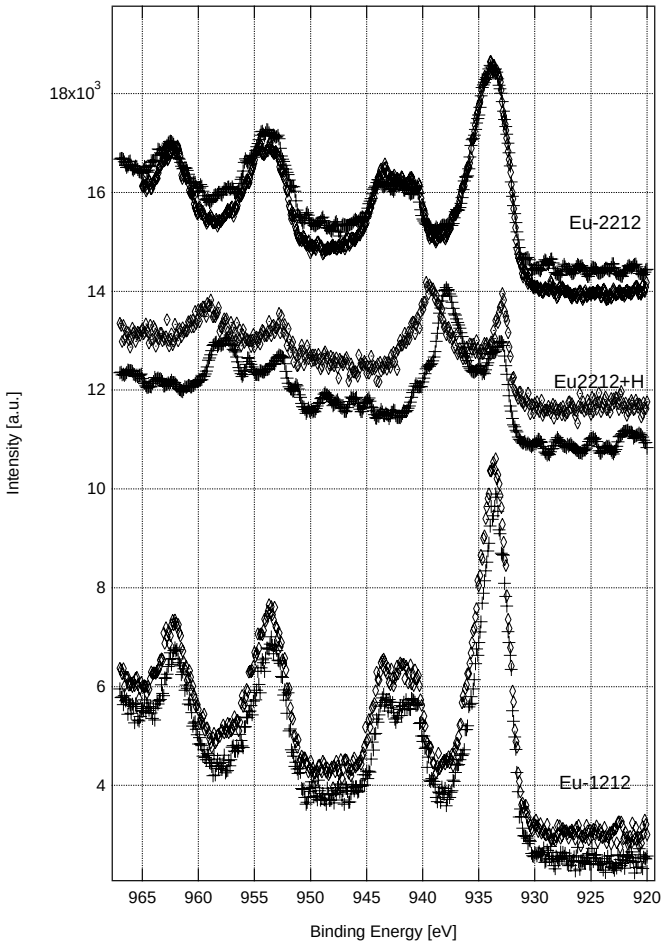

Fig. 3. Angle-integrated photoemission spectra taken using photon energy of 1486.6 eV. Spectra at room temperature (cross) and 80 K (diamond) illustrated. Top: Eu-2212; Middle: Eu-2212+H; Bottom: Eu-1212. Cu2p core levels and satellites visible.

and $SrRuO_3$ (lowest) spectra are presented. The $SrRuO_3$, Eu-1212, and Eu-2212 samples all exhibit a single Sr3d doublet; neither the intensity nor the binding energy shift with temperature. The ruthenocuprate samples exhibit a ~ 0.6 eV shift, to higher binding energy, of the doublet compared to $SrRuO_3$. The Eu-2212+H sample exhibits a shift of $\sim$1.8 eV, to higher binding energy, of the doublet compared to the $SrRuO_3$.

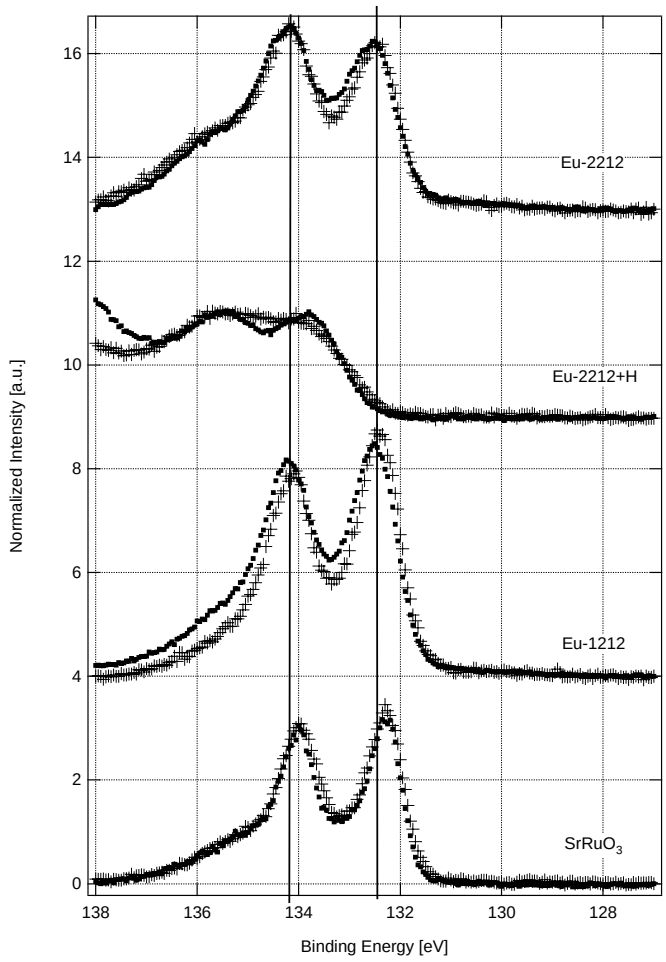

Fig. 4. Angle-integrated photoemission spectra taken using photon energy of 1486.6 eV. Spectra at room temperature (closed square) and 80 K (cross) illustrated. Top: Eu-2212; Second: Eu-2212+H; Third: Eu-1212; Bottom: $SrRuO_3$. Sr3*d* core level visible.

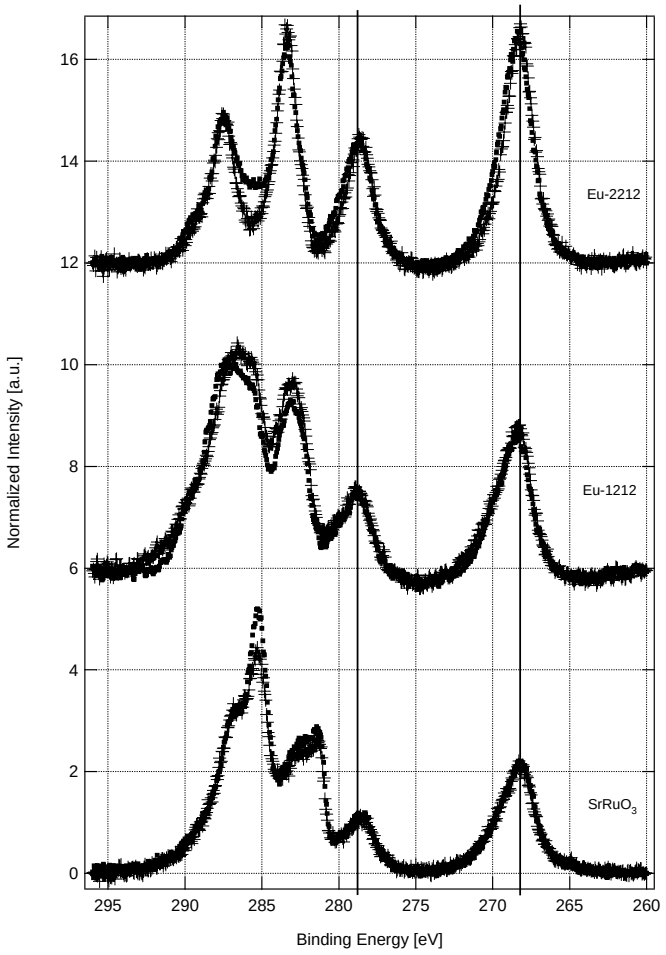

Fig. 5. Angle-integrated photoemission spectra taken using photon energy of 1486.6 eV. Spectra at room temperature (closed square) and 80 K (cross) illustrated. Top: Eu-2212; Middle: Eu-1212; Bottom: $SrRuO_3$. Sr3*p*, Ru3*d* and Eu4*p* core levels visible.

Sr3p, Ru3d, Eu4p region

Figure 5 illustrates the binding energy range of 260–296 eV, which includes the Sr3*p*, Ru3*d* and Eu4*p* core levels. Spectra include the Eu-1212 (top), Eu-2212 (second), ruthenocuprates, and $SrRuO_3$ (bottom). References [15–18] report Ru3*d* data [15] and interpret such data [16–18]. Our $SrRuO_3$ data are consistent with earlier reports; both a well screened and an unscreened final state doublet are visible. The well screened Ru3*d* doublet is at 281.0 eV and 285.2 eV, while the unscreened doublet is at 282.8 eV and 287.0 eV. Within the experimental error of ± 0.2 eV, these results are identical to those of reference [15], Figure 11. By contrast, the ruthenocuprate samples exhibit predominantly only the unscreened doublet. As reference [15] discusses, as the screened state becomes less likely, the transfer energy integral and the one electron bandwidth decrease. The data of Figure 5 indicate that the ruthenocuprate samples possess a more narrow bandwidth than does $SrRuO_3$. In addition, note that there is a shift of $\sim$1.0 eV of the Ru3*d* core levels for the ruthenocuprates compared to $SrRuO_3$. This compares to a shift of $\sim$0.6 eV for the Ru3*p* core levels, indicating a difference in the chemical potential of the ruthenocuprates compared to $SrRuO_3$.

Similarly, the Sr3*p* core levels for $SrRuO_3$ appear at binding energies identical to those reported earlier in reference [15]. Also, note that there is a small shift of the Sr3*p* core levels for the ruthenocuprate samples compared to $SrRuO_3$.

Cu3p region

Figure 6 illustrates the binding energy region from 70–90 eV for the three ruthenocuprate samples, including: Top: Eu-2212; Middle: Eu-2212+H; Bottom: Eu-2212. Cu3*p* core levels visible. Notice that the Cu3*p* peak appears at the same binding energy for all three, consistent with the Cu2*p* data of Figure 3. The metallic ruthenocuprate samples exhibit the same lineshape as reported previously by numerous investigators. However,

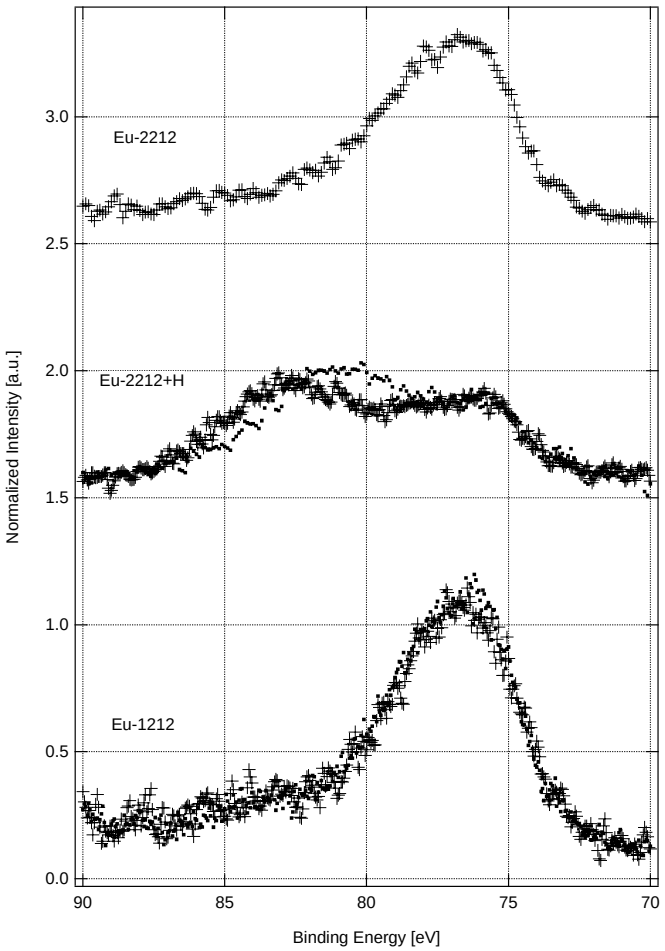

Fig. 6. Angle-integrated photoemission spectra taken using photon energy of 1486.6 eV. Spectra at room temperature (closed square) and 80 K (cross) illustrated. Top: Eu-2212; Middle: Eu-2212+H; Bottom: Eu-1212. Cu3*p* core levels visible.

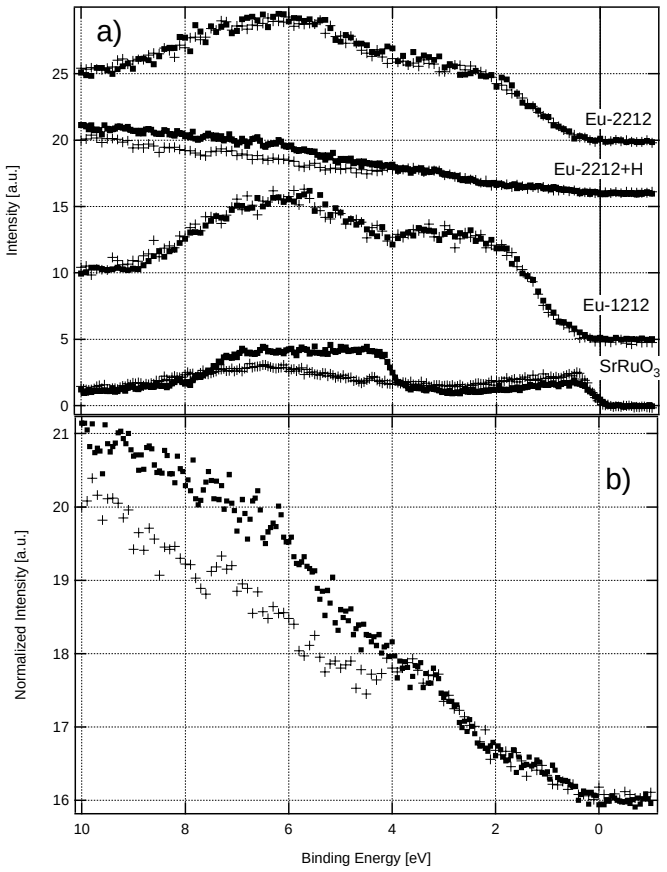

Fig. 7. (a) Angle-integrated photoemission spectra taken using photon energy of 1486.6 eV. Spectra at room temperature (closed square) and 80 K (cross) illustrated. Top: Eu-2212; Second: Eu-2212+H; Third: Eu-1212; Bottom: $SrRuO_3$. Valence band features visible. (b) Expanded view of valence band region for Eu-2212+H sample.

the hydrogen loaded ruthenocuprate sample exhibits a high binding energy satellite. This satellite has not been previously reported for Cu-containing compounds, and we tentatively assign it to a many-body response of the CuO_2 plane when we add hydrogen.

Valence band region

Figure 7a illustrates valence band spectra taken with 1486.6 eV photon energy, which favors Ru-*d* cross-section compared to O-*p*. The $SrRuO_3$ sample exhibits an energy-resolution limited feature at the chemical potential, and three main valence band features between 4–7.5 eV binding energy. The Eu-2212 ruthenocuprate samples exhibit significant differences compared to $SrRuO_3$ and to earlier work on cuprate samples [19–25]. None of the ruthenocuprate samples exhibit an strong spectral feature near the chemical potential. We reproduced this difference 10 times on several samples. Instead, there is a suppression of spectral intensity within ∼2 eV of the chemical potential. The metallic ruthenocuprates exhibit a strong feature at ∼3 eV binding energy that is absent for $SrRuO_3$. There are at least two other features in the valence band between 5–7.5 eV binding energy.

There are also significant differences between the metallic and Eu-2212+H ruthenocuprates. The spectral intensity between 0-2 eV is reduced by at least a factor of (×3) for the Eu-2212+H samples. We have displayed the data of Figure 7a with the same vertical scale. All valence band features for the Eu-2212+H samples are attenuated. In Figure 7b, we illustrated an expanded view of the Eu-2212+H valence band. While the Eu-2212+H valence band exhibits peaks in the density of states, it is worth emphasizing that the Eu-2212+H valence band does not resemble that of insulating cuprate samples, even when the same photon energy was used.

It is, however, important to note that the metallic and Eu-2212+H ruthenocuprates exhibit the same leading edge. We find no indication in the data of Figure 7a that there is a rigid shift of the leading edge

for the Eu-2212+H sample, as would be expected if there was an insulating bandgap. Instead, the leading edge behavior of all ruthenocuprate samples exhibit a loss of spectral intensity; this loss of intensity is reminiscent of a pseudogap such as has been reported for other lower dimensional materials [26–28].

Magnetic/superconducting properties

In this report, we have concentrated on the photoemission and electronic structure analysis of the ruthenocuprates. However, we present in Figure 8 a summary of our magnetic and superconducting measurements. The data of Figure 8 were measured in the zero field cooled process. Figure 8a illustrates the magnetization *versus* temperature of a Eu-1212 ruthenocuprate sample. The inset of Figure 8a illustrates the analogous measurement on $SrRuO_3$. Both Figure 8a and the inset were measured at 50 Oe. Note that the magnetization per mole for $SrRuO_3$ is $\sim(\times 30)$ larger than for Eu-1212. In addition, the $SrRuO_3$ exhibits a Curie temperature of ∼160 K while Eu-1212 exhibits a phase transition (ferromagnetic response) at ∼150 K (based on the maximum of the first derivative of magnetization *versus* temperature).

Figure 8b illustrates the magnetization *versus* temperature for a Eu-2212 ruthenocuprate sample in three circumstances: as-prepared; after hydrogen loading; after annealing in oxygen to remove the hydrogen. The inset illustrates the first derivative of the magnetization *versus* temperature curve for the as-prepared (ASP) sample. We note, as mentioned in the experimental section, that we deliberately loaded the samples with much more hydrogen than necessary to destroy the superconductivity. The ASP sample exhibits a phase transition at ∼88 K (see inset). Also, as highlighted in the inset by an arrow (↓), there is a smaller change at ∼122 K, which is a magnetic ordering of the Ru atom sublattice [2–5] The transition at 88 K is lower than the sample in Figure 8a, which contains no Ce. The ASP sample was measured in a 50 Oe field. The magnetization/mole/emu has a maximum of ∼3, which means that the magnetization per mole has a maximum of ∼150 emu/mole. This is a factor of $\sim(\times 5)$ larger than the ruthenocuprate sample of Figure 8a. It is particularly important to note the diamagnetic (superconducting) response of the ASP sample. The second derivative becomes negative at ∼65 K, and the magnetization itself becomes negative below 48 K. These data are most naturally interpreted as macroscopic superconductivity occurring at 48 K, and a competition between superconductivity and the other phase transition becoming evident at ∼65 K.

When hydrogen is loaded into the sample, the phase transition temperature shift to ∼180 K, higher that any metallic ruthenocuprate, or $SrRuO_3$. The data for the Eu-2212+H sample were taken at 35 Oe, so the maximum magnetization per mole is ∼210 emu/mole. Note that the magnetization remains positive for all temperatures measured, down to 5 K. The maximum magnetization per mole for the Eu-2212+H samples is higher than for the ASP sample, and $\sim(\times 8)$ higher than the ruthenocuprate in Figure 8a.

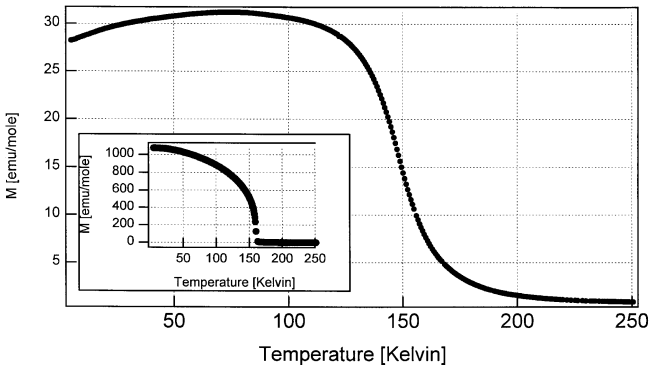

(a)

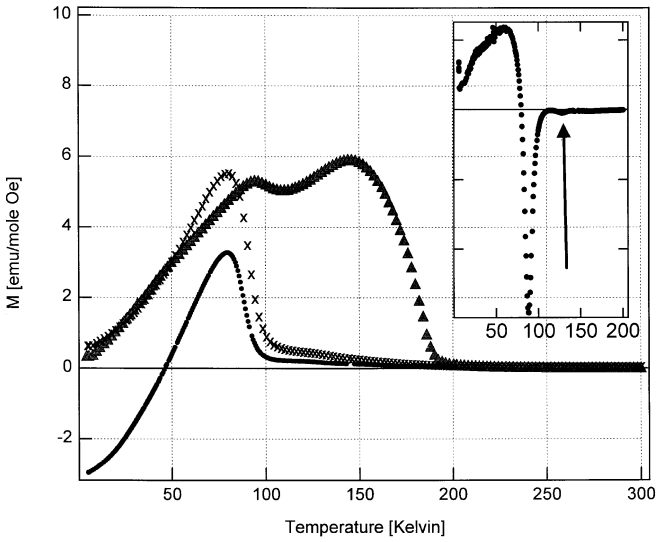

(b)

Fig. 8. (a) Magnetization per mole *versus* temperature for Eu-1212 sample, taken under zero field cooled conditions, with nominal (50 Oe) field. Inset: Analogous data for $SrRuO_3$ under same conditions. (b) Magnetization per mole per Oe *versus* temperature for Eu-2212 (closed square), Eu-2212+H (closed triangles), and regenerated E u-2212+H (×) samples. Inset: First derivative of Eu-2212 data in (b), with arrow highlighting change at ∼122 K.

We then took the Eu-2212+H sample and annealed it in oxygen at one atmosphere pressure (500 °C, 24 hours) to remove as much hydrogen as possible. We almost completely restored the original ASP sample properties. The phase transition temperature shifted back to ∼90 K, and the shape of the magnetization *versus* temperature is quite similar to the ASP sample: the temperature where $(\mathrm{d}M/\mathrm{d}T)$ becomes negative is also ∼90 K. We did not remove quite all the hydrogen, since the magnetization never becomes negative. Also, surprisingly, the magnetization/mole for the regenerated sample is virtually identical to that of the Eu-2212+H sample, although the phase transition temperature is much lower.

Discussion and conclusions

It is increasingly evident that the ruthenocuprates differ, chemically, electronically and magnetically, from either the ruthenate or cuprate parent compounds. We first discuss the effects of temperature, then the effects of stoichiometry on electronic properties, and finally the change of magnetic properties with stoichiometry. It is worth noting, at the beginning, the effects of adding hydrogen to the cuprates [29] or the ruthenates [30]. For the ruthenates, it seems that little hydrogen is incorporated. For the cuprates, the reports vary. Some report hydride formation, but there are also reports, such as reference [29], where the hydrogen appears not to form hydrides. The authors of reference [29] conclude that the hydrogen has two dominant effects. First, a magnetically ordered state forms, with a Néel temperature of 320 K; the exact nature of the magnetically ordered state was not elucidated. Second, the hydrogen acts to reduce the carrier concentration, in a manner similar to removing oxygen. There is a critical amount of hydrogen in $YBa_2Cu_3O_7H_x$: superconductivity disappears at $x \sim 0.2$, and some type of magnetic order appears above $x \sim 0.5$.

Let us first consider the changes with temperature. In an earlier report [31], we noted that the O1*s* X-ray photoemission data of $SrRuO_3$ and both superconducting and non-superconducting ruthenocuprates exhibit no shift of the O1*s* pre-edge feature in XPS at a binding energy of ∼528.5 eV. However, all exhibit a large shift with temperature of the feature at ∼532 eV. The shift is larger (∼2.1 eV) for the ruthenocuprates than for $SrRuO_3$ (∼1.1 eV). For the Eu-2212+H ruthenocuprates, the higher binding energy O1*s* feature shifts less (∼0.5 eV) with temperature. So there is a large shift of the occupied O1*s* features for the metallic samples, and a smaller change for the Eu-2212+H samples. By comparison, there is no shift with temperature for the cuprate samples in the same temperature range. In the cuprates, the peak at ∼532 eV can change for polycrystalline samples if there is a change of oxygen content. This means we cannot exclude a change in oxygen content accompanying adding hydrogen.

This shift of the higher binding energy O1*s* features for the metallic ruthenocuprate, or ruthenate, samples is the only change with temperature for the metallic samples. However, for the Eu-2212+H samples, as Table 2 illustrates, there are changes in the Cu2*p* and Eu3d*p* multiplet structure with temperature. In view of the changes in Table 2, it is tempting to ascribe the shifts with temperature to some rigid chemical shift. However, this is not the cause, since the Sr3*p* and Sr3*d* spectra for Eu-2212+H samples exhibit no shift with temperature. The data indicate that the multiplet is changing due to the ferromagnetic phase transition. This indicates that the unoccupied electronic states just above the chemical potential are affected by the ferromagnetic phase transition. We considered the possibility that there was a valence (charge) fluctuation at 80 K. We measured the Eu Mössbauer, but detected no change between 300 K and 80 K. Combined with the photoemission (Fig. 1), this means that the change in the multiplet structure with temperature is not due to any valence fluctuation. The shift of the Ru3*d* core level with temperature, along with the shift of the O1*s*, indicates that this shift is due to the ferromagnetic phase transition.

Table 2. Variation of core level features with temperature, between 300 K and 80 K, for the Eu-2212+H samples.

Core level	Variation with temperature
Eu3*d*	Shift of relative intensity of multiplet members
Cu2*p*	Intensity and binding energy of satellites

Table 3. Screening of core level(s), and valence, compared to $SrRuO_3$. For (Eu) and (Cu), the superconducting ruthenocuprate is the reference compound.

Element	WFM&SC	WFM	WFM&SC+H
Eu	same	same	same
Cu	same	same	same
Ru3*p*	+(0.6-1.0 eV)	+(0.6-1.0 eV)	+5 eV
Sr	+0.5-0.6 eV	+0.5-0.6 eV	+1.6 eV

There is one additional important consideration for these data: screening. $SrRuO_3$ exhibits metallic behavior; let us compare to this and the metallic cuprate benchmark compounds. At first, the results, summarized in Table 3, seem contradictory. Of the two planes that are nominally metallic, CuO_2 and RuO_2, the CuO_2 plane exhibits Cu2*p* and Cu3*p* core levels at virtually identical binding energies for all three ruthenocuprate members; the core level values are the same as both metallic and insulating cuprates. By contrast, the Ru core levels are affected by adding or removing hydrogen. Similarly, of the two nominally insulating planes, EuO and SrO, the (Eu) core levels are not changed by adding or removing hydrogen, while the (Sr) core levels are affected. At the same time, note that the EuO and CuO_2 planes exhibit marked changes in their many-body response when hydrogen is added or removed. Further, for the Eu-2212+H samples, the EuO and CuO_2 plane many-body responses change with temperature, as do the Ru core levels.

We draw the reader's attention to the shift of the (Ru) core levels for the metallic ruthenocuprate samples compared to $SrRuO_3$. Previous work by some of us (IF, IN) [7], using X-ray absorption, indicate that (Ru) in the metallic ruthenocuprate is pentavalent, while in $SrRuO_3$ (Ru) is tetravalent. The shift in (Ru) core levels listed in Table 3 is consistent with this difference in valence.

There remains in this picture one important experimental result: the effect of temperature for the Eu-2212+H ruthenocuprate samples. The Sr core levels do not change with temperature, while the Ru core levels and both the Eu and Cu multiplets do change. This indicates that the RuO_2 layers are directly involved in the energetics of the ferromagnetic phase transition. Further, the data indicate that the ferromagnetic phase transition affects electronic states of both Eu and Cu origin; the moment may be dominantly due to Ru, but the effect of the ferromagnetic phase transition extends to both Eu and Cu states. We speculate that the indirect effect on the EuO

and CuO_2 planes is *via* the internal magnetic field associated with the ferromagnetic state. Since the same changes are not observed for the metallic ruthenocuprates across the same ferromagnetic phase transition, we conclude that in the metallic ruthenocuprates, the mobile carriers screen out any effect of the ferromagnetic phase transition on the CuO_2 or EuO planes. Because the O1*s* features shift across the phase transition for both the metallic and Eu-2212+H ruthenocuprates, we conclude that the oxygen orbitals are directly involved in the phase transition. Since the oxygen states shift for both metallic and Eu-2212+H ruthenocuprates, while the ruthenium states shift only for the Eu-2212+H samples, we conclude that the mobile carriers, present for the metallic samples, are dominantly oxygen in nature. We infer that the nature of the ferromagnetic coupling is qualitatively different for the metallic and Eu-2212+H ruthenocuprates, with the coupling directly involving itinerant carriers for the metallic samples but only involving the localized Ru moments for the Eu-2212+H samples.

In summary, our results indicate that electronic states, dominantly oxygen, on the RuO_2 planes are directly involved in the energetics of the magnetic phase transition. The phase transition affects the core level multiplets on both the EuO and CuO_2 planes indirectly for the Eu-2212+H samples, probably due to the difference in screening between Eu-2212+H and hydrogen-free ruthenocuprates. The magnetic moment per volume changes markedly with hydrogen loading, indicating that both itinerant carriers and localized moments affect the magnetization properties. These data provide no further insight into why the magnetic ordering temperature increases for Eu-2212+H samples; this point has been discussed in other reports [1–9]. The data indicate that there are both Eu and Cu electronic states near the chemical potential; they affect the Eu and Cu core level multiplets but appear not to play a major role in the energetics of the magnetic phase transition.

We benefited from conversations with Clifford Olson. Financial support was provided by the U.S.-Israel Binational Science Foundation, EPFL and the Fonds National Suisse. The Wisconsin Synchrotron Radiation Center is supported financially by the U.S. NSF through grant DMR95-31009.

References

1. A. Ono, Jpn J. Phys. **34**, L1121 (1995).
2. I. Felner, U. Asaf, Y. Levi, O. Millo, Phys. Rev. B **55**, R3374 (1997).
3. I. Felner, U. Asaf, Y. Levi, O. Millo, Physica C **334**, 141 (2000).
4. I. Felner, U. Asaf, Phys. Rev. B **57**, 550 (1998).
5. I. Felner, U. Asaf, Physica C **292**, 97 (1997).
6. C. Bernhard, J.L. Tallon, Ch. Niedermayer, Th. Blasius, A. Golnik, E. Brücher, R.K. Kremer, D.R. Noakes, C.E. Stronach, E.J. Ansaldo, Phys. Rev. B **59**, 14099 (1999).
7. I. Felner, U. Asaf, C. Godart, E. Alleno, Physica B **259-261**, 703 (1999).
8. D.R. Pringle, J.L. Tallon, B.G. Walker, H.J. Trodahl, Phys. Rev. B **59**, R11679 (1999).
9. I. Felner, U. Asaf, S. Reich, Y. Tsabba, Physica C **311**, 163 (1999).
10. E.-J. Cho, S.-J. Oh, Phys. Rev. B **59**, R15613 (1999).
11. G.K. Wertheim, E.V. Sampathkumaran, C. Laubchat, G. Kaindl, Phys. Rev. B **31**, 6836 (1985).
12. E. Arenholz, K. Starke, G. Kaindl, P. Jensen, Phys. Rev. Lett. **80**, 2221 (1998).
13. S.-J. Oh (private communication).
14. S. Imada *et. al.* (unpublished).
15. P.A. Cox *et. al.* J. Phys. C **16**, 6221 (1983).
16. A. Kotani, Y. Toyazawa, J. Phys. Soc. Jpn **37**, 912 (1974).
17. P.A. Cox *et. al.*, in *Mixed Valence Compounds*, edited by D. Brown (Dordrecht, New York, 1980).
18. P.A. Cox, in *Proceedings X-80 Conference on Inner Shell and X-ray Physics of Atoms and Solids* (Plenum, New York, 1981).
19. A. Balzarotti, M. De Crescenzi, N. Motta, F. Patella, A. Sgarlata, Phys. Rev. B **38**, 6461 (1988).
20. P. Steiner, V. Kinsinger, I. Sanders, B. Siegwart, S. Hüfner, C. Politis, R. Hoppe, H.P. Müller, Z. Phys. B **67**, 497 (1987).
21. A. Fujimori, E. Takayama-Muromachi, Y. Uchida, B. Okai, Phys. Rev. B **35**, 8814 (1987).
22. D.D. Sarma, K. Sreedhar, P. Ganguly, C.N.R. Rao, Phys. Rev. B **36**, 2371 (1987).
23. Z.-X. Shen, J.W. Allen, J.J. Yeh, J.-S. Kang, W. Ellis, W. Spicer, I. Landau, M.B. Maple, Y.D. Dalichaouch, M.S. Torikachvilli, J.Z. Sun, T.H. Geballe, Phys. Rev. B **36**, 8414 (1987).
24. P. Steiner, S. Hüfner *et. al.*, Z. Phys. B **69**, 449 (1988).
25. D.D. Sarma, C.N.R. Rao, Solid State Commun. **65**, 47 (1988).
26. H. Ding *et al.*, Nature (London) **382**, 51 (1996).
27. A.G. Loeser *et al.*, Science **273**, 325 (1996).
28. F. Zwick, D. Jérome, G. Margaritondo, M. Onellion, J. Voit, M. Grioni, Phys. Rev. Lett. **81**, 2974 (1998).
29. Ch. Niedermayer *et. al.*, Phys. Rev. B **40**, 11386 (1987) and references therein.
30. I. Felner, unpublished.
31. B.H. Frazer *et. al.*, Phys. Rev. B **62**, 6716 (2000), and references therein.